

A Unified Approach to Superresolution and Multichannel Blind Deconvolution

Filip Šroubek, Gabriel Cristóbal, *Senior Member, IEEE*, and Jan Flusser, *Senior Member, IEEE*

Abstract—This paper presents a new approach to the blind deconvolution and superresolution problem of multiple degraded low-resolution frames of the original scene. We do not assume any prior information about the shape of degradation blurs. The proposed approach consists of building a regularized energy function and minimizing it with respect to the original image and blurs, where regularization is carried out in both the image and blur domains. The image regularization based on variational principles maintains stable performance under severe noise corruption. The blur regularization guarantees consistency of the solution by exploiting differences among the acquired low-resolution images. Several experiments on synthetic and real data illustrate the robustness and utilization of the proposed technique in real applications.

Index Terms—Image restoration, multichannel blind deconvolution, regularized energy minimization, resolution enhancement, superresolution.

I. INTRODUCTION

IMAGING devices have limited achievable resolution due to many theoretical and practical restrictions. An original scene with a continuous intensity function $o[x, y]$ warps at the camera lens because of the scene motion and/or change of the camera position. In addition, several external effects blur images: atmospheric turbulence, camera lens, relative camera-scene motion, etc. We will call these effects *volatile blurs* to emphasize their unpredictable and transitory behavior, yet we will assume that we can model them as convolution with an unknown point spread function (PSF) $v[x, y]$. This is a reasonable assumption if the original scene is flat and perpendicular to the optical axis. Finally, the CCD discretizes the images and produces digitized noisy image $g[i, j]$ (frame). We refer to $g[i, j]$ as a *low-resolution (LR) image*, since the spatial resolution is too low to capture all the details of the original scene. In conclusion, the acquisition model becomes

$$g[i, j] = D((v * W(o))[x, y]) + n[i, j] \quad (1)$$

Manuscript received October 30, 2006; revised May 23, 2007. This work was supported in part by the Czech Ministry of Education under the project 1M0572 (Research Center DAR), in part by the Academy of Sciences of the Czech Republic under the project AV0Z10750506-I055, in part by the bilateral project 2004CZ0009, and in part by the projects TEC2004-00834, TEC2005-24739-E, and PI040765. The associate editor coordinating the review of this manuscript and approving it for publication was Dr. Tamas Sziranyi.

F. Šroubek and J. Flusser are with the Institute of Information Theory and Automation, Academy of Sciences of the Czech Republic, Pod Vodárenskou věží 4, 18208 Prague 8, Czech Republic (e-mail: sroubekf@utia.cas.cz; flusser@utia.cas.cz).

G. Cristóbal is with the Instituto de Óptica, CSIC, Serrano 121, 28006 Madrid, Spain (e-mail: gabriel@optica.csic.es).

Color versions of one or more of the figures in this paper are available online at <http://ieeexplore.ieee.org>.

Digital Object Identifier 10.1109/TIP.2007.903256

where $n[i, j]$ is additive noise and W denotes the geometric deformation (warping). $D(\cdot) = S(g * \cdot)$ is the *decimation operator* that models the function of the CCD sensors. It consists of convolution with the *sensor PSF* $g[i, j]$ followed by the *sampling operator* S , which we define as multiplication by a sum of delta functions placed on an evenly spaced grid. The above model for one single observation $g[i, j]$ is extremely ill-posed. Instead of taking a single image we can take K ($K > 1$) images of the original scene and this way partially overcome the equivocation of the problem. Hence, we write

$$g_k[i, j] = D((v_k * W_k(o))[x, y]) + n_k[i, j] \quad (2)$$

where $k = 1, \dots, K$, and D remains the same in all the acquisitions. In the perspective of this multiframe model, the original scene $o[x, y]$ is a single input and the acquired LR images $g_k[i, j]$ are multiple outputs. The model is, therefore, called a single-input–multiple-output (SIMO) formation model. The upper part of Fig. 1 summarizes the multiframe LR acquisition process. To our knowledge, this is the most accurate, state-of-the-art model, as it takes all possible degradations into account. Several other authors, such as in [1]–[4], adopt this model, as well.

Superresolution (SR) is the process of combining a sequence of LR images in order to produce a higher resolution image or sequence. It is unrealistic to assume that the superresolved image can recover the original scene $o[x, y]$ exactly. A reasonable goal of SR is a discrete version of $o[x, y]$ that has a higher spatial resolution than the resolution of the LR images and that is free of the volatile blurs (deconvolved). In the paper, we will refer to this superresolved image as a *high resolution (HR) image* $f[i, j]$. The standard SR approach consists of subpixel registration, overlaying the LR images on an HR grid, and interpolating the missing values. The subpixel shift between images thus constitutes the essential assumption. We will demonstrate that assuming volatile blurs in the model explicitly brings about a more general and robust technique, with the subpixel shift being a special case thereof.

The acquisition model in (2) embraces three distinct cases frequently encountered in literature. First, if we want to resolve the geometric degradation W_k , we face a registration problem. Second, if the decimation operator D and the geometric transform W_k are not considered, we face a *multichannel* (or *multiframe*) *blind deconvolution* (MBD) problem. Third, if the volatile blur v_k is not considered or assumed known, and W_k is suppressed up to a subpixel translation, we obtain a classical SR formulation. In practice, it is crucial to consider all three cases at once. We are then confronted with a problem of *blind superresolution* (BSR), which is the subject of this investiga-

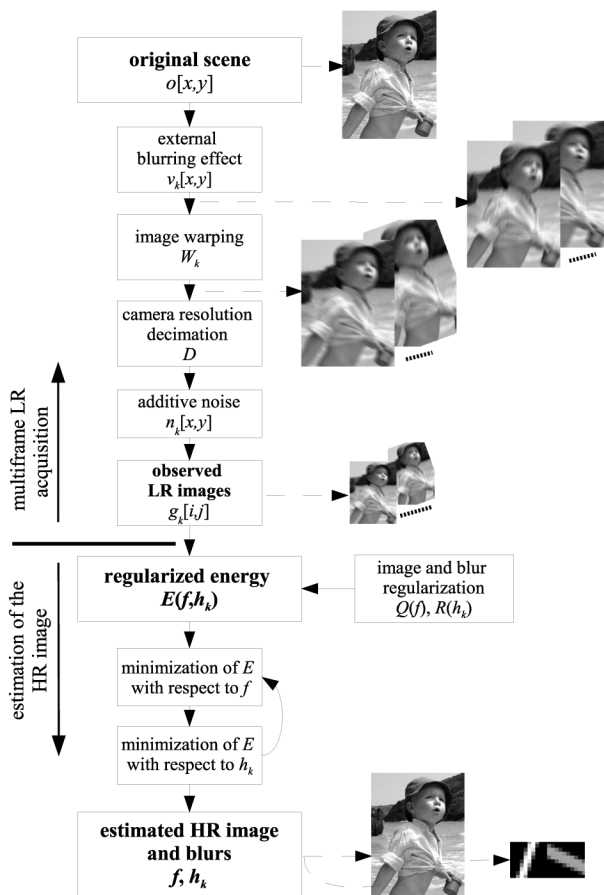


Fig. 1. (Top) Low-resolution acquisition and (bottom) reconstruction flow.

tion. The approach presented in this manuscript is one of the first attempts to solve BSR with only little prior knowledge.

Proper registration techniques can suppress large and complex geometric distortions (usually just up to a small between-image shift). There have been hundreds of methods proposed; see, e.g., [5] for a survey. In the rest of this paper, we will assume that the LR images are roughly registered and that W_k s reduce to small translations.

The MBD problem has recently attracted considerable attention. First blind deconvolution attempts were based on single-channel formulations, such as in [6]–[9]. Kundur *et al.* [10], [11] provide a good overview. The problem is extremely ill-posed in the single-channel framework and cannot be resolved in a fully blind form. These methods do not exploit the potential of the multichannel framework, because in the single-channel case missing information about the original image in one channel is not supplemented by information in the other channels. Research on intrinsically multichannel methods has begun fairly recently; refer to [12]–[16] for a survey and other references. Such MBD methods overpass the limitations of previous techniques and can recover the blurring functions from the degraded images alone. We further developed the MBD theory in [17] by proposing a blind deconvolution method for images, which might be mutually shifted by unknown vectors. To make this brief survey complete, we should not forget to mention a very challenging problem of shift-variant blind deconvolution, that was considered in [18] and [19].

A countless number of papers address the standard SR problem. A good survey can be found for example in [20] and [21]. Maximum likelihood, maximum *a posteriori* (MAP), the set theoretic approach using projection on convex sets, and fast Fourier techniques can all provide a solution to the SR problem. Earlier approaches assumed that subpixel shifts are estimated by other means. More advanced techniques, such as in [1], [2], and [4], include the shift estimation into the SR process. Other approaches focus on fast implementation [3], space-time SR [22] or SR of compressed video [2]. Most of the SR techniques assume *a priori* known blurs. However, in many cases, such as blurring due to camera motion, the blur can have a wild shape that is difficult to predict; see examples of real motion blurs in [23]. Authors in [24]–[26] proposed BSR that can handle parametric PSFs, i.e., PSFs modeled with one parameter. This restriction is unfortunately very limiting for most real applications. In [27], we extended our MBD method to BSR in an intuitive way but one can prove that this approach does not estimate PSFs accurately. The same intuitive approach was also proposed in [28]. To our knowledge, first attempts for theoretically correct BSR with an arbitrary PSF appeared in [29] and [30]. The interesting idea proposed therein is the conversion of the SR problem from SIMO to multiple input multiple output using so-called polyphase components. We will adopt the same idea here as well. Other preliminary results of the BSR problem with focus on fast calculation are given in [31], where the authors propose a modification of the Richardson–Lucy algorithm.

Current multiframe blind deconvolution techniques require no or very little prior information about the blurs, they are sufficiently robust to noise and provide satisfying results in most real applications. However, they can hardly cope with the decimation operator, which violates the standard convolution model. On the contrary, state-of-the-art SR techniques achieve remarkable results of resolution enhancement in the case of no blur. They accurately estimate the subpixel shift between images but lack any apparatus for calculating the blurs.

We propose a unifying method that simultaneously estimates the volatile blurs and HR image without any prior knowledge of the blurs and the original image. We accomplish this by formulating the problem as a minimization of a regularized energy function, where the regularization is carried out in both the image and blur domains. The image regularization is based on variational integrals, and a consequent anisotropic diffusion with good edge-preserving capabilities. A typical example of such regularization is total variation first proposed in [32]. However, the main contribution of this work lies in the development of the blur regularization term. We show that the blurs can be recovered from the LR images up to small ambiguity. One can consider this as a generalization of the results proposed for blur estimation in the case of MBD problems. This fundamental observation enables us to build a simple regularization term for the blurs even in the case of the SR problem. To tackle the minimization task, we use an alternating minimization approach (see Fig. 1), consisting of two simple linear equations.

The rest of the paper is organized as follows. Section II outlines the degradation model. In Section III, we present a procedure for volatile blur estimation. This effortlessly transforms into a regularization term of the BSR algorithm as described in Section IV. Finally, Section V illustrates applicability of the proposed method to real situations.

II. MATHEMATICAL MODEL

To simplify the notation, we will assume only images and PSFs with square supports. An extension to rectangular images is straightforward. Let $f[x, y]$ be an arbitrary discrete image of size $F \times F$, then \mathbf{f} denotes an image column vector of size $F^2 \times 1$ and $\mathbf{C}_A\{f\}$ denotes a matrix that performs convolution of f with an image of size $A \times A$. The convolution matrix can have a different output size. Adopting the Matlab naming convention, we distinguish two cases: “full” convolution $\mathbf{C}_A\{f\}$ of size $(F + A - 1)^2 \times A^2$ and “valid” convolution $\mathbf{C}_A^v\{f\}$ of size $(F - A + 1)^2 \times A^2$. In both cases, the convolution matrix is a Toeplitz-block-Toeplitz matrix. We will not specify dimensions of convolution matrices if it is obvious from the size of the right argument.

Let us assume we have K different LR frames $\{g_k\}$ (each of size $G \times G$) that represent degraded (blurred and noisy) versions of the original scene. Our goal is to estimate the HR representation of the original scene, which we denoted as the HR image f of size $F \times F$. The LR frames are linked with the HR image through a series of degradations similar to those between $o[x, y]$ and g_k in (2). First f is geometrically warped (\mathbf{W}_k), then it is convolved with a volatile PSF (\mathbf{V}_k) and finally it is decimated (\mathbf{D}). The formation of the LR images in vector-matrix notation is then described as

$$\mathbf{g}_k = \mathbf{D}\mathbf{V}_k\mathbf{W}_k\mathbf{f} + \mathbf{n}_k \quad (3)$$

where \mathbf{n}_k is additive noise present in every channel. The decimation matrix $\mathbf{D} = \mathbf{S}\mathbf{U}$ simulates the behavior of digital sensors by first performing convolution with the $U \times U$ sensor PSF (\mathbf{U}) and then downsampling (\mathbf{S}). The Gaussian function is widely accepted as an appropriate sensor PSF and it is also used here. Its justification is experimentally verified in [33]. A physical interpretation of the sensor blur is that the sensor is of finite size and it integrates impinging light over its surface. The sensitivity of the sensor is highest in the middle and decreases towards its borders with a Gaussian-like decay. Further, we assume that the subsampling factor (or SR factor, depending on the point of view), denoted by ε , is the same in both x and y directions. It is important to underline that ε is a user-defined parameter. In principle, \mathbf{W}_k can be a very complex geometric transform that must be estimated by image registration or motion detection techniques. We have to keep in mind that subpixel accuracy in \mathbf{g}_k s is necessary for SR to work. Standard image registration techniques can hardly achieve this and they leave a small misalignment behind. Therefore, we will assume that complex geometric transforms are removed in the preprocessing step and \mathbf{W}_k reduces to a small translation. Hence, $\mathbf{V}_k\mathbf{W}_k = \mathbf{H}_k$, where \mathbf{H}_k performs convolution with the shifted version of the volatile PSF v_k , and the acquisition model becomes

$$\mathbf{g}_k = \mathbf{D}\mathbf{H}_k\mathbf{f} + \mathbf{n}_k = \mathbf{S}\mathbf{U}\mathbf{H}_k\mathbf{f} + \mathbf{n}_k. \quad (4)$$

The BSR problem then adopts the following form: We know the LR images $\{g_k\}$ and we want to estimate the HR image f for the given \mathbf{S} and the sensor blur \mathbf{U} . To avoid boundary effects, we assume that each observation g_k captures only a part of f . Hence, \mathbf{H}_k and \mathbf{U} are “valid” convolution matrices $\mathbf{C}_F^v\{h_k\}$

and $\mathbf{C}_{F-H+1}^v\{u\}$, respectively. In general, the PSFs h_k are of different size. However, we postulate that they all fit into a $H \times H$ support.

In the case of $\varepsilon = 1$, the downsampling \mathbf{S} is not present and we face a slightly modified MBD problem that has been solved elsewhere [12], [17]. Here, we are interested in the case of $\varepsilon > 1$, when the downsampling occurs. Can we estimate the blurs as in the case $\varepsilon = 1$? The presence of \mathbf{S} prevents us from using the cited results directly. However, we will show that conclusions obtained for MBD apply here in a slightly modified form, as well.

III. RECONSTRUCTION OF VOLATILE BLURS

Estimation of blurs in the MBD case (no downsampling) attracted considerable attention in the past. A wide variety of methods were proposed, such as in [12] and [13], that provide a satisfactory solution. For these methods to work correctly, certain channel disparity is necessary. The disparity is defined as weak co-primeness of the channel blurs, which states that the blurs have no common factor except a scalar constant. In other words, if the channel blurs can be expressed as a convolution of two subkernels, then there is no subkernel that is common to all blurs. An exact definition of weakly co-prime blurs can be found in [13]. Many practical cases satisfy the channel co-primeness, since the necessary channel disparity is mostly guaranteed by the nature of the acquisition scheme and random processes therein. We refer the reader to [12] for a relevant discussion. This channel disparity is also necessary for the BSR case.

Let us first recall how to estimate blurs in the MBD case and then we will generalize the results for integer downsampling factors. For the time being, we will omit noise n , until Section IV, where we will address it appropriately.

A. MBD Case

The decimation matrix \mathbf{D} is not present in (4) and only convolution binds the input with the outputs. The acquisition model is of the SIMO type with one input channel f and K output channels g_k . Under the assumption of channel co-primeness, we can see that any two correct blurs h_i and h_j satisfy

$$g_i * h_j - g_j * h_i = 0. \quad (5)$$

There are $K(K - 1)/2$ such relations and they can be arranged into one system. Let us define

$$\mathcal{N}_{\text{MBD}} := (\mathbf{Z}_1^T \quad \dots \quad \mathbf{Z}_{K-1}^T)^T$$

$$\mathbf{Z}_i := \left(\begin{array}{cccccc} \mathbf{0} & \dots & \mathbf{0} & \mathbf{G}_{i+1} & -\mathbf{G}_i & \dots & \mathbf{0} \\ \vdots & \ddots & \vdots & \vdots & \vdots & \ddots & \vdots \\ \mathbf{0} & \dots & \mathbf{0} & \mathbf{G}_K & \mathbf{0} & \dots & -\mathbf{G}_i \end{array} \right) \quad (6)$$

$\underbrace{\hspace{10em}}_{i-1 \text{ blocks}} \quad \underbrace{\hspace{10em}}_{K-i+1 \text{ blocks}}$

for $i = 1, \dots, K - 1$, where $\mathbf{G}_i := \mathbf{C}_H^v\{g_i\}$. The complete system of relations (5) then takes the form

$$\mathcal{N}_{\text{MBD}}\mathbf{h} = \mathbf{0} \quad (7)$$

where $\mathbf{h} = [\mathbf{h}_1^T, \dots, \mathbf{h}_K^T]^T$. In most real situations, the correct blur size (we have assumed square size $H \times H$) is not known

in advance, and, therefore, we can generate the above equation for different blur dimensions $\hat{H}_1 \times \hat{H}_2$. The nullity (null-space dimension) of \mathcal{N}_{MBD} is exactly 1 for the correctly estimated blur size. By applying SVD (singular value decomposition), we recover precisely the blurs except for a scalar factor. One can eliminate this magnitude ambiguity by stipulating that $\sum_{x,y} h_k[x,y] = 1$, which is a common brightness preserving assumption. For the underestimated blur size, the above equation has no solution. If the blur size is overestimated, then $\text{nullity}(\mathcal{N}_{\text{MBD}}) = (\hat{H}_1 - H + 1)(\hat{H}_2 - H + 1)$.

B. BSR Case

Before we proceed, it is necessary to define precisely the sampling matrix \mathbf{S} . Let \mathbf{S}_1^ε denote a 1-D sampling matrix, where ε is the integer subsampling factor. Each row of the sampling matrix is a unit vector whose nonzero element is at such position that, if the matrix multiplies an arbitrary vector b , the result of the product is every ε th element of b . If the vector length is M then the size of the sampling matrix is $(M/\varepsilon) \times M$. If M is not divisible by ε , we can pad the vector with an appropriate number of zeros to make it divisible. A 2-D sampling matrix is defined by

$$\mathbf{S}^\varepsilon := \mathbf{S}_1^\varepsilon \otimes \mathbf{S}_1^\varepsilon \quad (8)$$

where \otimes denotes the matrix direct product (Kronecker product operator). Note that the transposed matrix $(\mathbf{S}^\varepsilon)^T$ behaves as an upsampling operator that interlaces the original samples with $(\varepsilon - 1)$ zeros.

A naive approach, as proposed in [27] and [28], is to modify (7) for the MBD case by applying downsampling, $\mathcal{N}_{\text{BSR}} = \mathcal{N}_{\text{MBD}}[\mathbf{I}_K \otimes \mathbf{S}^\varepsilon \mathbf{U}]$, and formulating the problem as

$$\min_{\mathbf{h}} \|\mathcal{N}_{\text{BSR}} \mathbf{h}\|^2 \quad (9)$$

where \mathbf{I}_K is the $K \times K$ identity matrix. One can easily verify that the condition in (5) is not satisfied for the BSR case as the presence of downsampling operators violates the commutative property of convolution. Even more disturbing is the fact that minimizers of (9) do not have to correspond to the correct blurs. We are going to show that if one uses a slightly different approach, reconstruction of the volatile PSFs h_k is possible even in the BSR case. However, we will see that some ambiguity in the solution of h_k is inevitable.

First, we need to rearrange the acquisition model (4) and construct from the LR images g_k a convolution matrix \mathcal{G} with a predetermined nullity. Then, we take the null space of \mathcal{G} and construct a matrix \mathcal{N} , which will contain the correct PSFs h_k in its null space.

Let $E \times E$ be the size of “nullifying” filters η_{kn} . (The meaning of this name will be clear later). Define $\mathcal{G} := [\mathbf{G}_1, \dots, \mathbf{G}_K]$, where $\mathbf{G}_k := \mathbf{C}_E^v\{g_k\}$ are “valid” convolution matrices. Assuming no noise, we can express \mathcal{G} in terms of f , u , and h_k as

$$\mathcal{G} = \mathbf{S}^\varepsilon \mathbf{F} \mathbf{U} \mathcal{H} \quad (10)$$

where

$$\mathcal{H} := [\mathbf{C}_{\varepsilon E}\{h_1\}(\mathbf{S}^\varepsilon)^T, \dots, \mathbf{C}_{\varepsilon E}\{h_K\}(\mathbf{S}^\varepsilon)^T] \quad (11)$$

$$\mathbf{U} := \mathbf{C}_{\varepsilon E+H-1}\{u\} \text{ and } \mathbf{F} := \mathbf{C}_{\varepsilon E+H+U-2}\{f\}.$$

The convolution matrix \mathcal{U} has more rows than columns, and, therefore, it is of full column rank (see proof in [12] for general convolution matrices). We assume that $\mathbf{S}^\varepsilon \mathbf{F}$ has full column rank as well. This is almost certainly true for real images if \mathbf{F} has at least ε^2 times more rows than columns. Thus, $\text{Null}(\mathcal{G}) \equiv \text{Null}(\mathcal{H})$ and the difference between the number of columns and rows of \mathcal{H} bounds from below the null space dimension, i.e.,

$$\text{nullity}(\mathcal{G}) \geq KE^2 - (\varepsilon E + H - 1)^2. \quad (12)$$

Setting $N := KE^2 - (\varepsilon E + H - 1)^2$ and $\mathbf{N} := \text{Null}(\mathcal{G})$, we visualize the null space as

$$\mathbf{N} = \begin{bmatrix} \mathbf{n}_{1,1} & \dots & \mathbf{n}_{1,N} \\ \vdots & \ddots & \vdots \\ \mathbf{n}_{K,1} & \dots & \mathbf{n}_{K,N} \end{bmatrix} \quad (13)$$

where \mathbf{n}_{kn} is the vector representation of the nullifying filter η_{kn} of size $E \times E$, $k = 1, \dots, K$ and $n = 1, \dots, N$. The filters η_{kn} are made of values of \mathcal{G} 's null space and that is where their name comes from. Let $\tilde{\eta}_{kn}$ denote upsampled η_{kn} by factor ε , i.e., $\tilde{\eta}_{kn} := (\mathbf{S}^\varepsilon)^T \eta_{kn}$. Then, we define

$$\mathcal{N} := \begin{bmatrix} \mathbf{C}_H\{\tilde{\eta}_{1,1}\} & \dots & \mathbf{C}_H\{\tilde{\eta}_{K,1}\} \\ \vdots & \ddots & \vdots \\ \mathbf{C}_H\{\tilde{\eta}_{1,N}\} & \dots & \mathbf{C}_H\{\tilde{\eta}_{K,N}\} \end{bmatrix} \quad (14)$$

and conclude that

$$\mathcal{N} \mathbf{h} = \mathbf{0} \quad (15)$$

where $\mathbf{h}^T = [\mathbf{h}_1, \dots, \mathbf{h}_K]$. We have arrived to an equation that is of the same form as (7) in the MBD case. Here, we have the solution to the blur estimation problem for the BSR case. However, since \mathbf{S}^ε is involved, ambiguity of the solution is higher. Without proofs (for the sake of simplicity) we provide the following statements. For the correct blur size, $\text{nullity}(\mathcal{N}) = \varepsilon^4$. For the underestimated blur size, (15) has no solution. For the overestimated blur size $\hat{H}_1 \times \hat{H}_2$, $\text{nullity}(\mathcal{N}) = \varepsilon^2(\hat{H}_1 - H + \varepsilon)(\hat{H}_2 - H + \varepsilon)$. The conclusion may seem to be pessimistic. For example, for $\varepsilon = 2$ the nullity is at least 16, and for $\varepsilon = 3$ the nullity is already 81.

To shed more light on the above discussion about the nullity we have visualized the null space of \mathcal{N} in Fig. 2. We convolved an image with six different 8×8 PSFs (the first PSF is in the top of Fig. 2), downsampled the blurred images with factor 2, and then constructed \mathcal{N} from the images following the above derivation. We know that in this case 16 independent vectors span the null space of \mathcal{N} and their arbitrary linear combination is a solution to (15). One such configuration of 16 independent vectors, where only the first PSF is extracted from each, is shown in the bottom of Fig. 2 arranged in a 4×4 table. One can see that the recovered PSFs contain parts of the original PSF and we have got four distinct parts each shifted to four different positions. Section IV will show that \mathcal{N} plays an important role in the restoration algorithm as a consistency term and its ambiguity is not a serious drawback.

It is interesting to note that a similar derivation is possible for rational SR factors $\varepsilon = p/q$. We downsample the LR im-

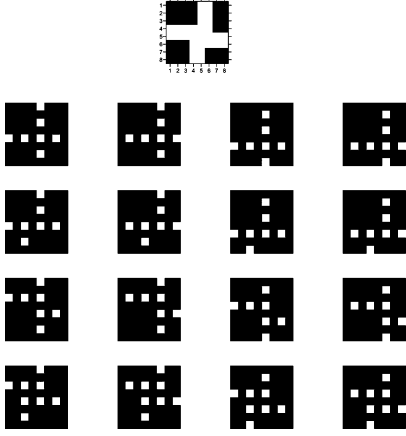


Fig. 2. Visualization of \mathcal{N} 's null space for $\varepsilon = 2$. (Top) Original 8×8 PSF and (bottom) one example of 16 PSFs that span the null space of \mathcal{N} . Proper linear combination of these 16 PSFs gives the original PSF.

ages with the factor q , thereby creating q^2K images and apply thereon the above procedure for the SR factor p .

Another consequence of the above derivation is the minimum necessary number of LR images for the blur reconstruction to work. The condition of the \mathcal{G} nullity in (12) implies that the minimum number is $K > \varepsilon^2$. For example, for $\varepsilon = 3/2$, 3 LR images are sufficient; for $\varepsilon = 2$, we need at least 5 LR images to perform blur reconstruction. An intuitive explanation is that ε^2 input images are necessary for the SR problem to get a fully determined system of equations and additional input images are for the PSF estimation.

IV. BLIND SUPERRESOLUTION

In order to solve the BSR problem, i.e., determine the HR image f and volatile PSFs h_k , we adopt an approach of minimizing a regularized energy function. This way, the method will be less vulnerable to noise and better posed. The energy consists of three terms and takes the form

$$E(\mathbf{f}, \mathbf{h}) = \sum_{k=1}^K \|\mathbf{D}\mathbf{H}_k \mathbf{f} - \mathbf{g}_k\|^2 + \alpha Q(\mathbf{f}) + \beta R(\mathbf{h}). \quad (16)$$

The first term measures the fidelity to the data and emanates from our acquisition model (4). The remaining two are regularization terms with positive weighting constants α and β that attract the minimum of E to an admissible set of solutions. The form of E very much resembles the energy proposed in [17] for MBD. Indeed, this should not come as a surprise since MBD and SR are related problems in our formulation.

Regularization $Q(\mathbf{f})$ is a smoothing term of the form

$$Q(\mathbf{f}) = \mathbf{f}^T \mathbf{L} \mathbf{f} \quad (17)$$

where \mathbf{L} is a high-pass filter. A common strategy is to use convolution with the Laplacian for \mathbf{L} , which in the continuous case corresponds to $Q(f) = \int |\nabla f|^2$. Recently, variational integrals $Q(f) = \int \phi(|\nabla f|)$ were proposed, where ϕ is a strictly convex, nondecreasing function that grows at most linearly. Examples of $\phi(s)$ are s (total variation), $\sqrt{1+s^2} - 1$ (hypersurface minimal function), $\log(\cosh(s))$, or nonconvex functions, such as

$\log(1+s^2)$, $s^2/(1+s^2)$ and $\arctan(s^2)$ (Mumford–Shah functional). The advantage of the variational approach is that it behaves as anisotropic diffusion. While in smooth areas it has the same isotropic behavior as the Laplacian, it also preserves edges in images. The disadvantage is that it is highly nonlinear. To overcome this difficulty one must use, e.g., the half-quadratic algorithm [34]. For the purpose of our discussion, it suffices to state that after discretization we arrive again at (17), where this time \mathbf{L} is a positive semidefinite block tridiagonal matrix constructed of values depending on the gradient of f . The rationale behind the choice of $Q(f)$ is to constrain the local spatial behavior of images; it resembles a Markov random field. Some global constraints may be more desirable but are difficult (often impossible) to define, since we develop a general method that should work with any class of images.

The PSF regularization term $R(\mathbf{h})$ directly follows from the conclusions of the previous section. Since the matrix \mathcal{N} in (14) contains the correct PSFs h_k in its null space, we define the regularization term as a least-squares fit

$$R(\mathbf{h}) = \|\mathcal{N}\mathbf{h}\|^2 = \mathbf{h}^T \mathcal{N}^T \mathcal{N} \mathbf{h}. \quad (18)$$

If one replaces \mathcal{N} with \mathcal{N}_{BSR} , we have the naive approach. The product $\mathcal{N}^T \mathcal{N}$ is a positive semidefinite matrix. More precisely, R is a consistency term that binds volatile PSFs and prevents them from moving freely and, unlike the fidelity term [the first term in (16)], it is based solely on the observed LR images. A good practice is to include with a small weight a smoothing term $\mathbf{h}^T \mathbf{L} \mathbf{h}$ in $R(\mathbf{h})$. This is especially useful in the case of less noisy data in order to overcome the higher nullity of \mathcal{N} .

The complete energy then takes the form

$$E(\mathbf{f}, \mathbf{h}) = \sum_{k=1}^K \|\mathbf{D}\mathbf{H}_k \mathbf{f} - \mathbf{g}_k\|^2 + \alpha \mathbf{f}^T \mathbf{L} \mathbf{f} + \beta_1 \|\mathcal{N}\mathbf{h}\|^2 + \beta_2 \mathbf{h}^T \mathbf{L} \mathbf{h}. \quad (19)$$

Energy E as a function of both variables \mathbf{f} and \mathbf{h} , is not convex due to convolution in the first term. On the other hand, the energy function is convex with respect to \mathbf{f} if \mathbf{h} is fixed and it is convex with respect to \mathbf{h} if \mathbf{f} is fixed. The minimization sequence $(\mathbf{f}^m, \mathbf{h}^m)$ can, thus, be built by alternating between two minimization subproblems. This procedure is called alternating minimizations (AM) and the advantage lies in its simplicity. For each subproblem a unique minimum exists that can be easily calculated. Derivatives w.r.t. \mathbf{f} and \mathbf{h} must be zero at the minima, which, in this case, leads to solving a set of simple linear equations. In conclusion, starting with some initial \mathbf{h}^0 the two iterative steps are

$$\begin{aligned} \text{Step 1)} \quad \mathbf{f}^m &= \arg \min_{\mathbf{f}} E(\mathbf{f}, \mathbf{h}^m) \Rightarrow \frac{\partial E}{\partial \mathbf{f}} = \mathbf{0} \\ &\Leftrightarrow \left(\sum_{k=1}^K \mathbf{H}_k^T \mathbf{D}^T \mathbf{D} \mathbf{H}_k + \alpha \mathbf{L} \right) \mathbf{f} \\ &= \sum_{k=1}^K \mathbf{H}_k^T \mathbf{D}^T \mathbf{g}_k \\ \text{Step 2)} \quad \mathbf{h}^{m+1} &= \arg \min_{\mathbf{h}} E(\mathbf{f}^m, \mathbf{h}) \Rightarrow \frac{\partial E}{\partial \mathbf{h}} = \mathbf{0} \\ &\Leftrightarrow ([\mathbf{I}_K \otimes \mathbf{F}^T \mathbf{D}^T \mathbf{D} \mathbf{F}] + \beta_1 \mathcal{N}^T \mathcal{N} + \beta_2 \mathbf{L}) \mathbf{h} \\ &= [\mathbf{I}_K \otimes \mathbf{F}^T \mathbf{D}^T] \mathbf{g} \end{aligned} \quad (20)$$

$$= [\mathbf{I}_K \otimes \mathbf{F}^T \mathbf{D}^T] \mathbf{g} \quad (21)$$

where $\mathbf{F} := \mathbf{C}_H^v\{f\}$, $\mathbf{g} := [\mathbf{g}_1^T, \dots, \mathbf{g}_K^T]^T$ and m is the iteration step. The AM approach is a variation on the steepest-descent algorithm. The search space is a concatenation of the blur subspace and the image subspace. The algorithm first descends in the image subspace and after reaching the minimum, i.e., $\partial E/\partial \mathbf{f} = \mathbf{0}$, it advances in the blur subspace in the direction $\partial E/\partial \mathbf{h}$ orthogonal to the previous one, and this scheme repeats. Due to the coupling of the variables by convolution, we cannot guarantee in theory that the global minimum is reached but thorough testing indicates good convergence properties of the algorithm for many real problems.

Convergence may further improve if we add feasible regions for the HR image and PSFs specified as lower and upper bounds constraints. To solve step 1, we use the method of conjugate gradients (function *cgs* in standard Matlab) and then adjust the solution \mathbf{f}^m to contain values in the admissible range, typically, the range of values of \mathbf{g} . It is common to assume that PSF is positive and preserves image brightness, i.e., $h_k \geq 0$ and $\sum_{x,y} h_k[x,y] = 1$. We can, therefore, restrict the intensity values of PSFs between 0 and 1. In order to enforce the bounds in step 2, we solve (21) as a constrained minimization problem (function *fmincon* in Matlab Optimization Toolbox v.3) rather than using the projection as in step 1. Constrained minimization problems are more computationally demanding but we can afford it in this case since the size of \mathbf{h} is much smaller than the size of \mathbf{f} .

The weighting constants α and β_i depend on the level of noise. If noise increases, α and β_2 should increase, and β_1 should decrease. One can use parameter estimation techniques, such as cross-validation [24] or expectation maximization [35], to determine the correct weights. However, in our experiments, we set the values manually according to a visual assessment. If the iterative algorithm begins to amplify noise, we have underestimated the noise level. On the contrary, if the algorithm begins to segment the image, we have overestimated the noise level.

V. EXPERIMENTS

This section consists of two parts. In the first one, a set of experiments on synthetic data evaluate performance of the BSR algorithm with respect to the SR factor and compare the reconstruction quality with other methods mentioned below under different levels of noise. The second part demonstrates the applicability of the proposed method to real data.

In all the experiments the sensor blur is fixed and set to a Gaussian function of standard deviation $\sigma = 0.34$ (relative to the scale of LR images). One should underline that the proposed BSR method is fairly robust to the choice of the Gaussian variance, since it can compensate for insufficient variance by automatically including the missing factor of Gaussian functions in the volatile blurs.

Another potential pitfall that we have to take into consideration is a feasible range of SR factors. Theoretically there are no limitations on the upper bound of the SR factor. However, practical reasons impose limits. As the SR factor ε increases, we need more LR images ($K > \varepsilon^2$). The increasing number of LR images negatively affects the stability of BSR, since in real scenarios perturbations of the acquisition model occur, which

disrupts the minimization scheme. SR factors beyond 2.5 are, thus, rare in real applications. A more elaborated discussion on fundamental limits of SR algorithms is given in [36]. In addition, rational SR factors p/q , where p and q are incommensurable and large regardless of the effective value of ε , also make the BSR algorithm unstable. It is the numerator p that determines the internal SR factor used in the algorithm. Hence, we limit ourselves to ε between 1 and 2.5, such as $3/2$, $5/3$, 2, etc., which is sufficient in most practical applications.

A. Simulated Data

First, let us demonstrate the BSR performance with a simple experiment. An 175×175 image in Fig. 3(a) blurred with six masks in Fig. 3(b) and downsampled with factor 2 gives six LR images. Using the LR images as an input, we estimated the original HR image with the proposed BSR algorithm for $\varepsilon = 1.5$ and 2. Fig. 4 summarizes obtained results in their original size. One can see, that for $\varepsilon = 1.5$ [Fig. 4(b)], the reconstruction is good but some details, such as the shirt texture, are still fuzzy. For the SR factor 2, the reconstructed image in Fig. 4(c) is almost perfect as most of the high-frequency information of the original image is correctly recovered.

Next, we evaluate noise robustness of the proposed BSR and compare it with other two methods: interpolation technique and state-of-the-art SR method. The former technique consists of the MBD method proposed in [17] followed by standard bilinear interpolation resampling. The MBD method first removes volatile blurs and then the interpolation of the deconvolved image achieves the desired spatial resolution. The latter method, which we will call herein a “standard SR algorithm,” is a MAP formulation of the SR problem proposed, e.g., in [1] and [2]. This method uses a MAP framework for the joint estimation of image registration parameters (in our case only translation) and the HR image, assuming only the sensor blur (\mathbf{U}) and no volatile blurs. For an image prior, we use edge preserving Huber Markov random fields [33].

In the case of BSR, Section III shows that two distinct approaches exist for the blur estimation. Either we use the naive approach in (9) that directly utilizes the MBD formulation, or we apply the intrinsically SR approach given in (15). Depending on the approach, we use either \mathcal{N}_{BSR} or \mathcal{N} in the blur consistency term $R(\mathbf{h})$ in the AM algorithm.

Altogether we have, thus, four distinct methods for comparison: standard SR approach, MBD with interpolation, BSR with naive blur regularization and BSR with intrinsic blur regularization. The experimental setup was the following. First, we generated six random motion blurs of size 4×4 . Then we generated six LR images from the original HR image in Fig. 3(a) using the blurs and the downsampling factor of 2, and added white Gaussian noise with different SNR from 50 to 1 dB. The signal-to-noise ratio is defined as $\text{SNR} = 10 \log(\sigma_f^2/\sigma_n^2)$, where σ_f and σ_n are the image and noise standard deviations, respectively. We repeated the whole procedure ten times for different realizations of noise. For each set of six LR images, the four methods were applied one by one. Parameters of each method were chosen to minimize the mean square error of the HR estimate. Fig. 5 summarizes the

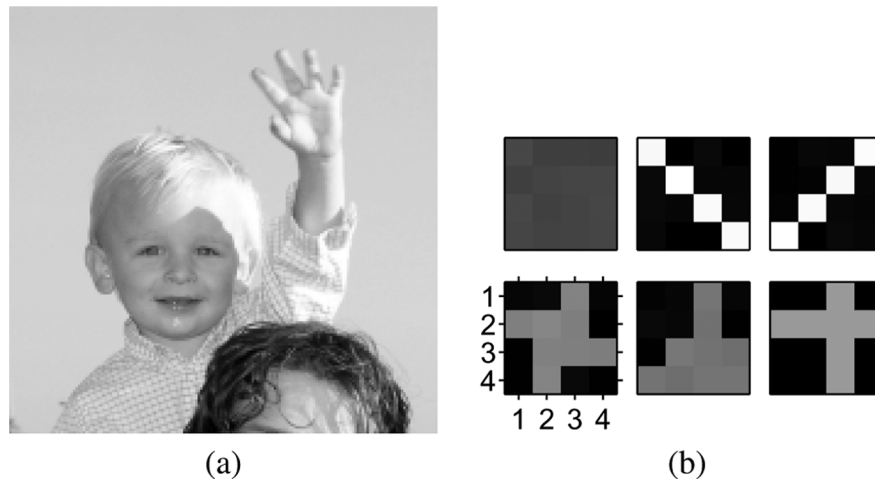


Fig. 3. Simulated data: (a) original 175×175 image; (b) six 4×4 volatile PSFs used to blur the original image.

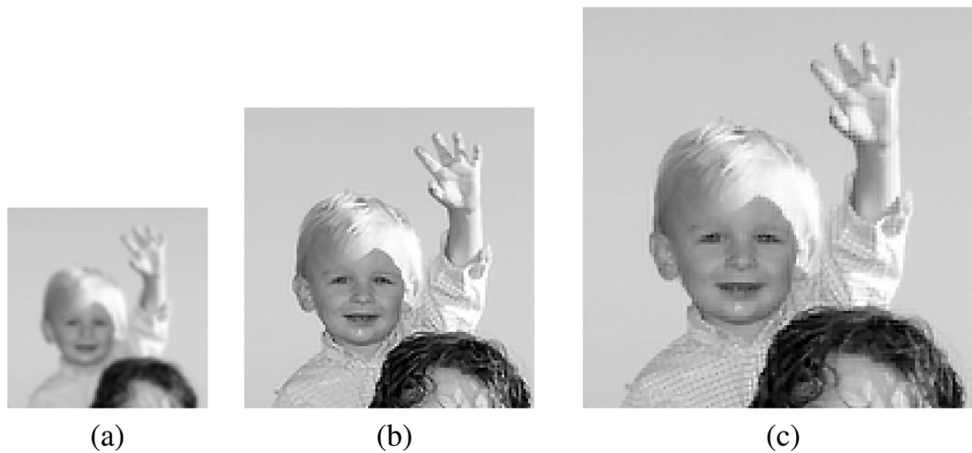


Fig. 4. BSR of simulated data: (a) one of six LR images with the downsampling factor 2; (b) BSR for $\varepsilon = 1.5$; (c) BSR for $\varepsilon = 2$. The shirt texture is not yet visible for the SR factor 1.5 but becomes well reconstructed for the SR factor 2. On the other hand, face features probably lack very small details, and there is no visible improvement between 1.5 and 2.

obtained results in terms of peak signal to noise ratio defined as $\text{PSNR}(\hat{\mathbf{f}}) = 10 \log(\text{span}(\mathbf{f})^2 / \|\hat{\mathbf{f}} - \mathbf{f}\|^2 / F^2)$, where $\hat{\mathbf{f}}$ is the estimate of the original HR image \mathbf{f} , and $\text{span}(\mathbf{f})$ denotes the span of gray-level values in the original image, typically 255.

The standard SR method gives the poorest performance, since it lacks any apparatus for removing volatile blurs. MBD with interpolation removes blurs in the LR domain, which accounts for better performance. However, the best performance is apparent for the proposed BSR method, which accomplishes SR and blind deconvolution in the HR domain. The shape of the blur consistency term $R(\mathbf{h})$ plays its role, as well. In the case of the naive consistency term (\mathcal{N}_{BSR}), estimated blurs are less accurate. This leads to tiny artifacts in the HR image and a small performance drop. On the other hand, the blur consistency term with \mathcal{N} provides the most accurate estimations and outperforms all the other methods. For low SNR, all the tested methods tend to give similar results in the PSNR perspective and advantages of the proposed BSR method are less evident. Thus, for very noisy images (below 20 dB), it is sufficient to perform MBD with simple interpolation than to apply advanced SR methods, since MBD is definitely faster and the results look similar due to noise. The level of noise depends on the amount of light during

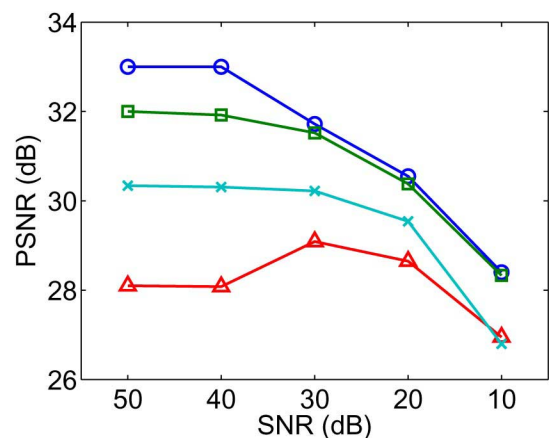


Fig. 5. Performance of the BSR algorithm and the other two methods under different levels of noise: (\circ) BSR using \mathcal{N} in the blur consistency term $R(\mathbf{h})$; (\square) BSR using \mathcal{N}_{BSR} ; (\times) MBD with bilinear interpolation; (\triangle) standard SR method. Note that the proposed BSR outperforms any other method but as the noise level increases its supremacy becomes less evident.

acquisition and also on the quality of sensors. In our experience, most regular digital cameras have SNR around 50 dB, but

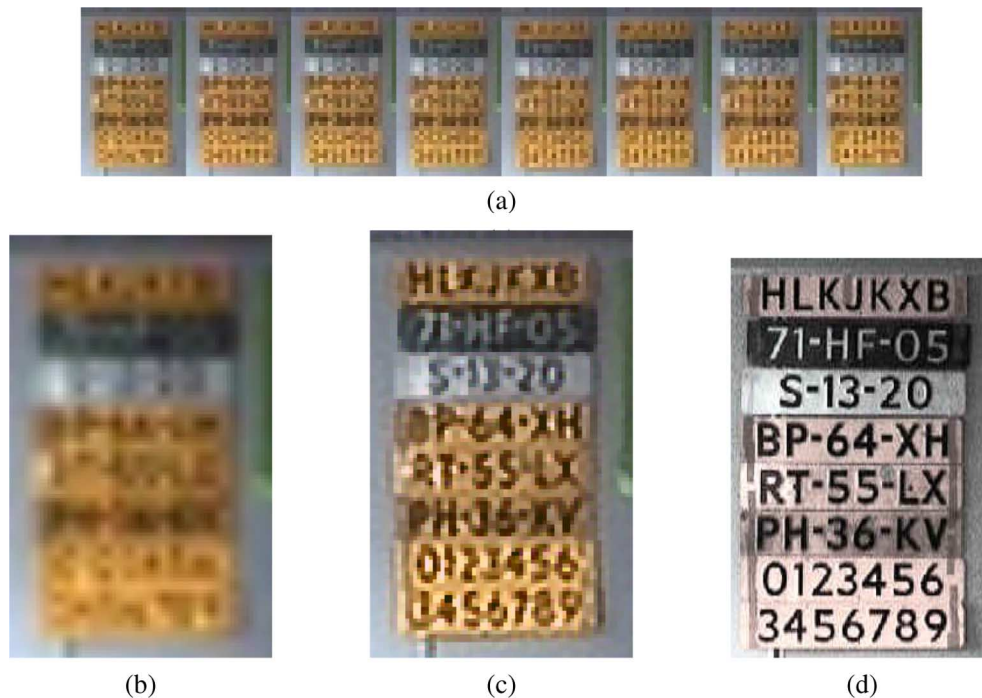


Fig. 6. Reconstruction of images acquired with a camcorder ($\varepsilon = 2.5$): (a) eight LR frames created from a short video sequence captured with the camcorder and displayed in their original size; (b) bilinear interpolation of one LR frame; (c) BSR estimate of the HR frame; (d) original HR frame.

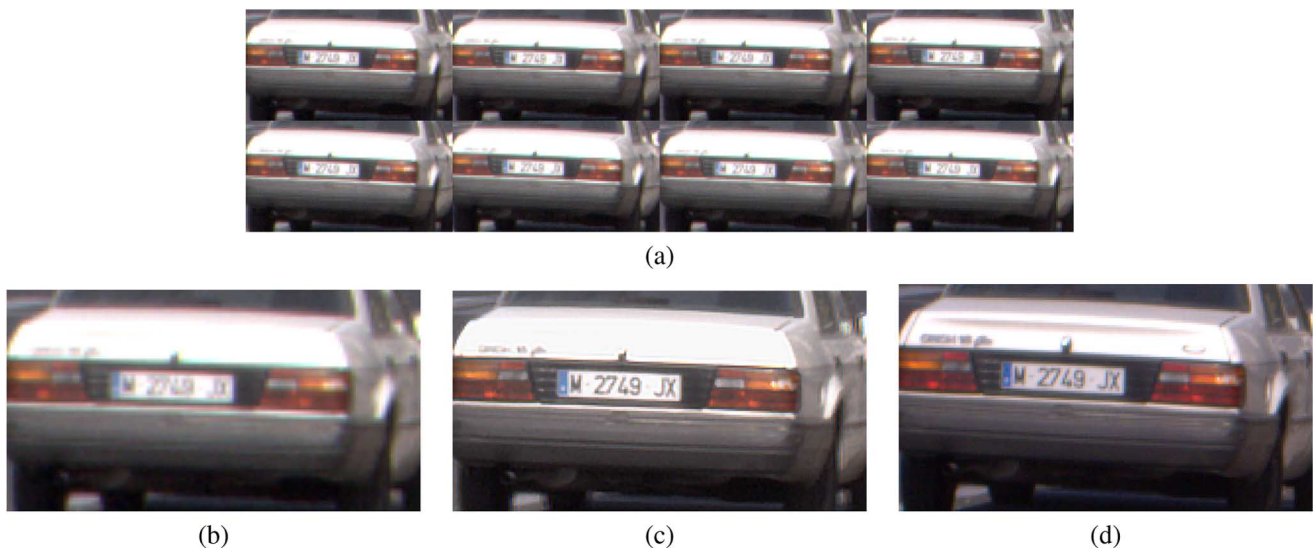


Fig. 7. Reconstruction of images acquired with a digital camera ($\varepsilon = 2$): (a) eight LR acquired shot with the digital camera and displayed in their original size; (b) bilinear interpolation of one LR image; (c) BSR estimate of the HR image; (d) image taken by the same camera but with optical zoom. The BSR algorithm achieves reconstruction comparable to the image with optical zoom.

with decreasing light, it can drop down to 30 dB. Webcameras have in general lower SNR around 30 dB, even in moderate light conditions.

B. Real Data

The next three experimental settings come from a license plate recognition task and they demonstrate the true power of the BSR algorithm. We used data from two different acquisition devices: camcorder and digital camera. The camcorder was Sony Digital Handycam and the digital camera was 5-Mpixel Olympus C5050Z equipped with $3\times$ optical zoom. In order to

work with color images, we extended the proposed BSR method by utilizing color TV [37] instead of standard TV in image regularization and by assuming the same blurring in all three color channels.

In the first scenario, we used a short video sequence provided by Dr. Z. Geradts from the Netherlands Forensic Institute (available at forensic.to/superresolution.htm). The video sequence was acquired with the camcorder and was artificially downsampled with factor 10. We extracted 16 frames from the downsampled video, of which eight are in Fig. 6(a), and applied the proposed BSR algorithm with the SR factor of 2.5. Fig. 6(b)

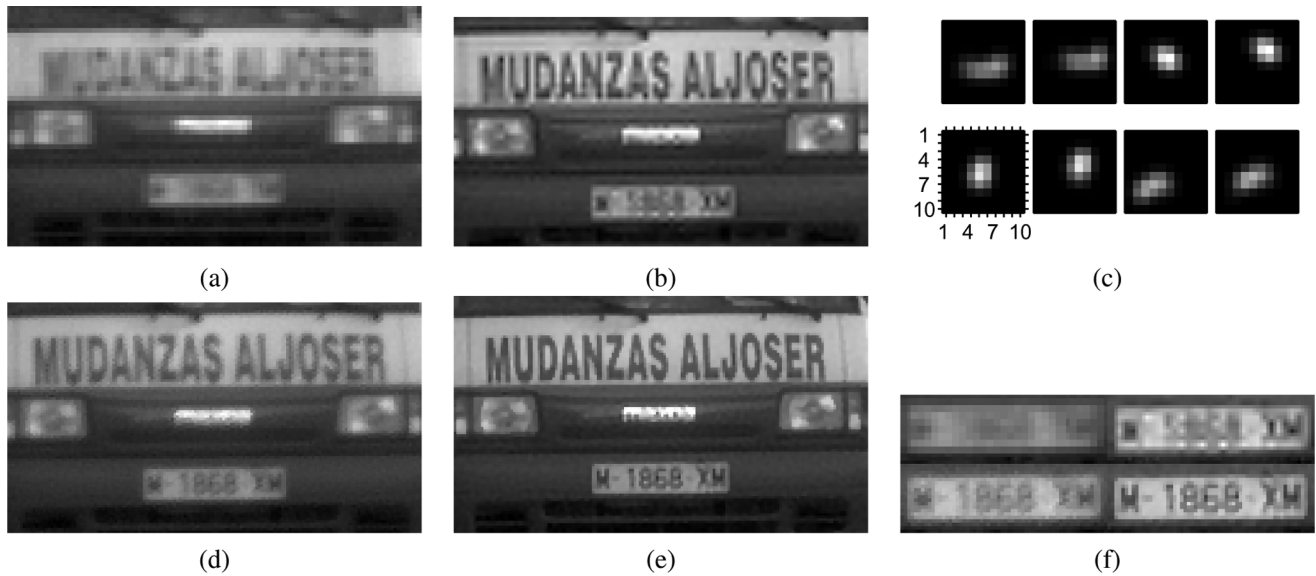


Fig. 8. License-plate recognition ($\varepsilon = 2$): (a) one of eight LR images acquired with a digital camera (zero-order interpolation); (b) MBD followed by bilinear interpolation; (c) PSFs estimated by the proposed BSR; (d) standard SR algorithm; (e) proposed BSR algorithm; (f) closeups of the images (a) and (b) on top and (d) and (e) on bottom. Note that only the BSR result (e) reconstructs the car brand name in such a way that we can deduce that it was a “Mazda” car.

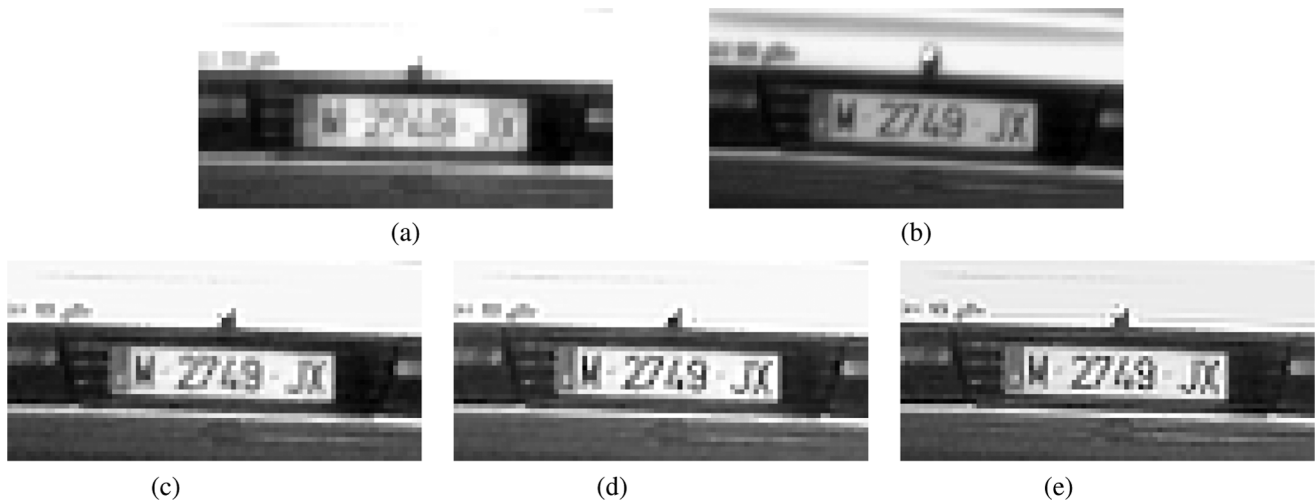


Fig. 9. Performance of the BSR algorithm with respect to the number of LR images ($\varepsilon = 1.5$). (a) One of eight LR images of size 40×70 , zero-order interpolation. (b) Image acquired with optical zoom $1.5 \times$, which plays the role of “ground truth.” The proposed BSR algorithm using (c) 3, (d) 4, and (e) 8 LR images.

shows the first LR frame bilinearly interpolated to have the size of HR images. The HR frame estimated by BSR is in Fig. 6(c), and the original undecimated HR frame is in Fig. 6(d). The obtained result remarkably well recovers letters and numbers on the license plates.

In the second scenario, we used the digital camera and took eight photos of a stalled car, registered the photos with cross-correlation and cropped each to a 100×50 rectangle. All eight cuttings printed in their original size (no interpolation), including one image enlarged with bilinear interpolation, are in Fig. 7(a) and (b). We set the desired SR factor to 2 and applied BSR. In order to better assess the obtained results, we took one additional image with optical zoom set close to $2 \times$. This image served as the ground truth; see Fig. 7(d). The proposed BSR method returned a well reconstructed HR image [Fig. 7(c)], which surpasses the image acquired with the optical zoom.

The third experimental setting consisted of a car moving towards a hand-held digital camera. We took four consecutive color images with the camera, and using both green channels (color image in digital cameras are made of two green channels and one red and one blue channel), we generated altogether eight LR images. The images were roughly registered with cross-correlation and cropped each to a 90×50 rectangle. One such image is in Fig. 8(a). We set the SR factor to 2 and applied different reconstruction techniques. The MBD with interpolation method [Fig. 8(b)] reconstructed the banner satisfactory, yet the license plate is not legible, since it contains tiny details that are beyond the resolution of LR images. The standard SR approach in Fig. 8(d) gives moderate results. The proposed BSR method in Fig. 8(e) outperforms all the other techniques and provides a sharp HR image. The PSFs estimated by BSR are in Fig. 8(c). Note that every second PSF is a shifted

version of the previous one, which was expected, since green channels in digital cameras are shifted diagonally by 1 pixel in each direction. For better visual comparison closeups of one of the input LR image and three reconstructed HR images appear in Fig. 8(f).

When dealing with real data, one cannot expect that the performance will increase without limits as the number of available LR images increases. At a certain point possible discrepancies between the measured data and our mathematical model take over, and the estimated HR image does not improve any more or it can even worsen. We conducted several experiments on real data (short shutter speed and motionless objects) with different SR factors and number of LR images K . See the results of one such experiment in Fig. 9 for $\varepsilon = 1.5$ and the number of LR images ranging from 3 to 8. A small improvement is apparent between using 3 and 4 LR images; compare Fig. 9(c) and (d). However, the result obtained with all eight images in Fig. 9(e) shows a very little improvement. We deduce that for each SR factor exists an optimal number of LR images that is close to the minimum necessary number. Therefore, in practice, we recommend to use the minimum or close to minimum number of LR images for the given SR factor.

VI. CONCLUSION

We have shown that the SR problem permits a stable solution, even in the case of unknown blurs. The fundamental idea is to split radiometric deformations into sensor and volatile parts and assume that only the sensor part is known. We can then construct a convex functional using the observed LR images and observe that the volatile part minimizes this functional. Due to the presence of resolution decimation, the functional is not strictly convex and reaches its minimum on a subspace that depends on the integer SR factor. We have also extended our conclusions to rational factors. To achieve robust solution, we have adopted the regularized energy minimization approach. The proposed BSR method goes far beyond the standard SR techniques. The introduction of volatile blurs makes the method particularly appealing to real situations. While reconstructing the blurs, we estimate not only subpixel shifts but also any possible blurs imposed by the acquisition process. To our knowledge, this is one of the first methods that performs deconvolution and resolution enhancement simultaneously.

REFERENCES

- [1] R. Hardie, K. Barnard, and E. Armstrong, "Joint map registration and high-resolution image estimation using a sequence of undersampled images," *IEEE Trans. Image Process.*, vol. 6, no. 12, pp. 1621–1633, Dec. 1997.
- [2] C. Segall, A. Katsaggelos, R. Molina, and J. Mateos, "Bayesian resolution enhancement of compressed video," *IEEE Trans. Image Process.*, vol. 13, no. 7, pp. 898–911, Jul. 2004.
- [3] S. Farsiu, M. Robinson, M. Elad, and P. Milanfar, "Fast and robust multiframe super resolution," *IEEE Trans. Image Process.*, vol. 13, no. 10, pp. 1327–1344, Oct. 2004.
- [4] N. Woods, N. Galatsanos, and A. Katsaggelos, "Stochastic methods for joint registration, restoration, and interpolation of multiple undersampled images," *IEEE Trans. Image Process.*, vol. 15, no. 1, pp. 201–213, Jan. 2006.
- [5] B. Zitová and J. Flusser, "Image registration methods: A survey," *Image Vis. Comput.*, vol. 21, pp. 977–1000, 2003.
- [6] R. Legendijk, J. Biemond, and D. Boeke, "Identification and restoration of noisy blurred images using the expectation-maximization algorithm," *IEEE Trans. Acoust. Speech Signal Process.*, vol. 38, no. 7, pp. 1180–1191, Jul. 1990.
- [7] S. Reeves and R. Mersereau, "Blur identification by the method of generalized cross-validation," *IEEE Trans. Image Process.*, vol. 1, no. 7, pp. 301–311, Jul. 1992.
- [8] T. Chan and C. Wong, "Total variation blind deconvolution," *IEEE Trans. Image Process.*, vol. 7, no. 3, pp. 370–375, Mar. 1998.
- [9] M. Haindl, "Recursive model-based image restoration," in *Proc. 15th Int. Conf. Pattern Recognition*, 2000, vol. III, pp. 346–349.
- [10] D. Kundur and D. Hatzinakos, "Blind image deconvolution," *IEEE Signal Process. Mag.*, vol. 13, no. 3, pp. 43–64, May 1996.
- [11] D. Kundur and D. Hatzinakos, "Blind image deconvolution revisited," *IEEE Signal Process. Mag.*, vol. 13, no. 6, pp. 61–63, Nov. 1996.
- [12] G. Hari Kumar and Y. Bresler, "Perfect blind restoration of images blurred by multiple filters: Theory and efficient algorithms," *IEEE Trans. Image Process.*, vol. 8, no. 2, pp. 202–219, Feb. 1999.
- [13] G. Giannakis and R. Heath, "Blind identification of multichannel FIR blurs and perfect image restoration," *IEEE Trans. Image Process.*, vol. 9, no. 11, pp. 1877–1896, Nov. 2000.
- [14] H.-T. Pai and A. Bovik, "On eigenstructure-based direct multichannel blind image restoration," *IEEE Trans. Image Process.*, vol. 10, no. 10, pp. 1434–1446, Oct. 2001.
- [15] G. Panci, P. Campisi, S. Colonnese, and G. Scarano, "Multichannel blind image deconvolution using the bussgang algorithm: Spatial and multiresolution approaches," *IEEE Trans. Image Process.*, vol. 12, no. 11, pp. 1324–1337, Nov. 2003.
- [16] F. Šroubek and J. Flusser, "Multichannel blind iterative image restoration," *IEEE Trans. Image Process.*, vol. 12, no. 9, p. 1094, Sep. 2003.
- [17] F. Šroubek and J. Flusser, "Multichannel blind deconvolution of spatially misaligned images," *IEEE Trans. Image Process.*, vol. 14, no. 7, pp. 874–883, Jul. 2005.
- [18] Y.-L. You and M. Kaveh, "Blind image restoration by anisotropic regularization," *IEEE Trans. Image Process.*, vol. 8, no. 3, pp. 396–407, Mar. 1999.
- [19] A. Rajagopalan and S. Chaudhuri, "An MRF model-based approach to simultaneous recovery of depth and restoration from defocused images," *IEEE Trans. Pattern Anal. Mach. Intell.*, vol. 21, no. 7, pp. 577–589, Jul. 1999.
- [20] S. Park, M. Park, and M. Kang, "Super-resolution image reconstruction: A technical overview," *IEEE Signal Process. Mag.*, vol. 20, no. 3, pp. 21–36, Mar. 2003.
- [21] S. Farsui, D. Robinson, M. Elad, and P. Milanfar, "Advances and challenges in super-resolution," *Int. J. Imag. Syst. Technol.*, vol. 14, no. 2, pp. 47–57, Aug. 2004.
- [22] E. Shechtman, Y. Caspi, and M. Irani, "Space-time super-resolution," *IEEE Trans. Pattern Anal. Mach. Intell.*, vol. 27, no. 4, pp. 531–545, Apr. 2005.
- [23] M. Ben-Ezra and S. Nayer, "Motion-based motion deblurring," *IEEE Trans. Pattern Anal. Mach. Intell.*, vol. 26, no. 6, pp. 689–698, Jun. 2004.
- [24] N. Nguyen, P. Milanfar, and G. Golub, "Efficient generalized cross-validation with applications to parametric image restoration and resolution enhancement," *IEEE Trans. Image Process.*, vol. 10, no. 9, pp. 1299–1308, Sep. 2001.
- [25] N. Woods, N. Galatsanos, and A. Katsaggelos, "EM-based simultaneous registration, restoration, and interpolation of super-resolved images," in *Proc. IEEE Int. Conf. Image Processing*, 2003, vol. 2, pp. 303–306.
- [26] D. Rajan and S. Chaudhuri, "Simultaneous estimation of super-resolved scene and depth map from low resolution defocused observations," *IEEE Trans. Pattern Anal. Mach. Intell.*, vol. 25, no. 9, pp. 1102–1117, Sep. 2003.
- [27] F. Šroubek and J. Flusser, "Resolution enhancement via probabilistic deconvolution of multiple degraded images," *Pattern Recognit. Lett.*, vol. 27, pp. 287–293, Mar. 2006.
- [28] Y. Chen, Y. Luo, and D. Hu, "A general approach to blind image super-resolution using a PDE framework," *Proc. SPIE*, vol. 5960, pp. 1819–1830, 2005.
- [29] Wirawan, P. Duhamel, and H. Maitre, "Multi-channel high resolution blind image restoration," in *Proc. IEEE ICASSP*, 1999, pp. 3229–3232.
- [30] A. Yagle, "Blind superresolution from undersampled blurred measurements," in *Proc. Advanced Signal Processing Algorithms, Architectures, and Implementations XIII*, 2003, vol. 5205, pp. 299–309.
- [31] D. Biggs, C. L. Wang, T. Holmes, and A. Khodjakov, "Subpixel deconvolution of 3D optical microscope imagery," *Proc. SPIE*, vol. 5559, pp. 369–380, Oct. 2004.

- [32] L. Rudin, S. Osher, and E. Fatemi, "Nonlinear total variation based noise removal algorithms," *Phys. D*, vol. 60, pp. 259–268, 1992.
- [33] D. Capel, *Image Mosaicing and Super-Resolution*. New York: Springer, 2004.
- [34] G. Aubert and P. Kornprobst, *Mathematical Problems in Image Processing*. New York: Springer Verlag, 2002.
- [35] R. Molina, M. Vega, J. Abad, and A. Katsaggelos, "Parameter estimation in Bayesian high-resolution image reconstruction with multisensors," *IEEE Trans. Image Process.*, vol. 12, no. 12, pp. 1655–1667, Dec. 2003.
- [36] Z. Lin and H.-Y. Shum, "Fundamental limits of reconstruction-based superresolution algorithms under local translation," *IEEE Trans. Pattern Anal. Mach. Intell.*, vol. 26, no. 1, pp. 83–97, Jan. 2004.
- [37] D. Tschumperlé and R. Deriche, "Diffusion PDE's on vector-valued images," *IEEE Signal Process. Mag.*, vol. 19, no. 5, pp. 16–25, Sep. 2002.



Filip Šroubek received the M.Sc. degree in computer science from the Czech Technical University, Prague, Czech Republic, in 1998, and the Ph.D. degree in computer science from the Charles University, Prague, in 2003.

From 2004 to 2006, he was in a postdoctoral position at the Instituto de Optica, CSIC, Madrid, Spain. He is currently with the Institute of Information Theory and Automation and also with the Institute of Photonics and Electronics, Academy of Sciences of the Czech Republic. He is an author of two book

chapters and over 25 journal and conference papers on image fusion, blind deconvolution, superresolution, and related topics.



Gabriel Cristóbal (SM'96) received the M.Sc. and Ph.D. degrees in telecommunication engineering from the Universidad Politecnica de Madrid, Madrid, Spain, in 1979 and 1986, respectively.

He was Visiting Scholar at the International Computer Science Institute and an Associate Researcher at the University of California, Berkeley, from 1989 to 1992. He is currently a Research Scientist with the Instituto de Optica, Spanish Council for Scientific Research, Madrid. His current research interests are joint representations, vision modeling, resolution

enhancement, and image compression.



Jan Flusser (SM'03) received the M.Sc. degree in mathematical engineering from the Czech Technical University, Prague, Czech Republic, in 1985, the Ph.D. degree in computer science from the Czechoslovak Academy of Sciences in 1990, and the D.Sc. degree in technical cybernetics in 2001.

Since 1985, he has been with the Institute of Information Theory and Automation, Academy of Sciences of the Czech Republic, Prague. From 1995 to 2006, he held the position of Head of the Department of Image Processing. In 2007, he was appointed

to Director of the Institute. Since 1991, he has also been affiliated with the Charles University, Prague, and the Czech Technical University, Prague, where he teaches courses on digital image processing and pattern recognition. He has been a Full Professor since 2004. His current research interests include all aspects of digital image processing and pattern recognition, namely 2-D object recognition, moment invariants, blind deconvolution, image registration, and image fusion. He has authored and coauthored more than 150 research publications in these areas.